磁性奈米脂粒之製作與其溫控藥物制放特性之研究

Iron-Oxide Embedded Solid Lipid Nanoparticles for Magnetically Controlled Drug Delivery

本研究開發的磁性奈米脂粒在常溫下為固體，其中包覆藥物與加熱用的氧化鐵微粒，利用外加的交流磁場可使氧化鐵微粒產熱，熔化脂質並促成藥物的快速釋放；透過表面修飾加強氧化鐵微粒在脂質中的溶解度，並以高壓均質製程生成奈米脂粒；已完成的雛形可在二十分鐘內升溫十度，釋放出百分之三十五的含藥量。

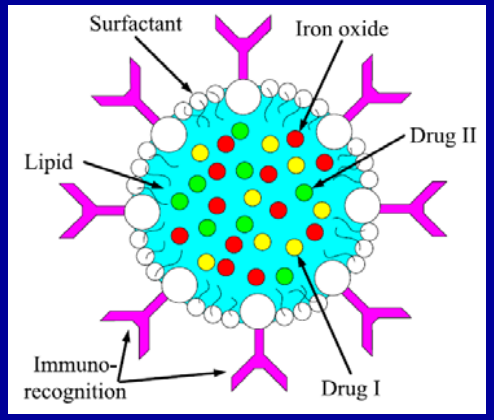

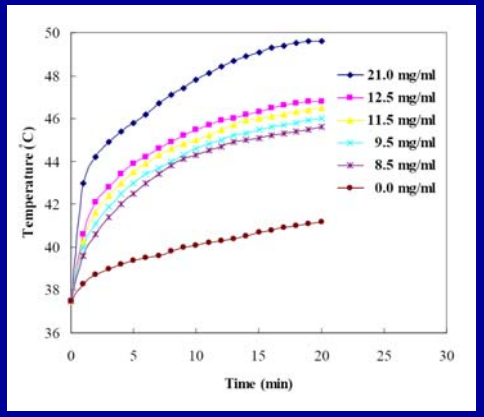

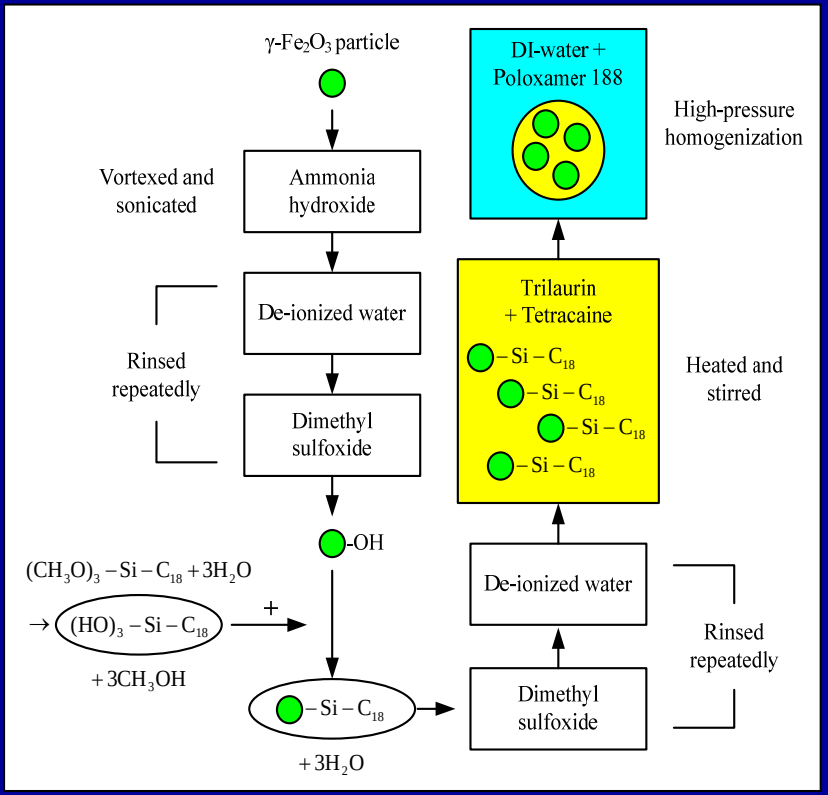

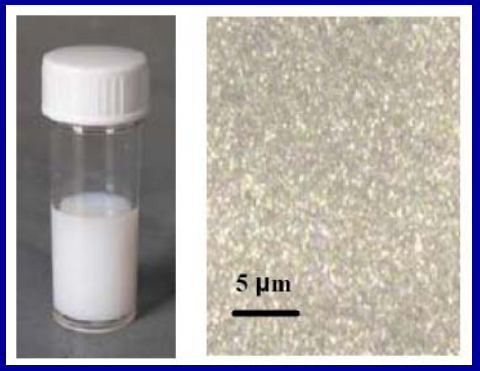

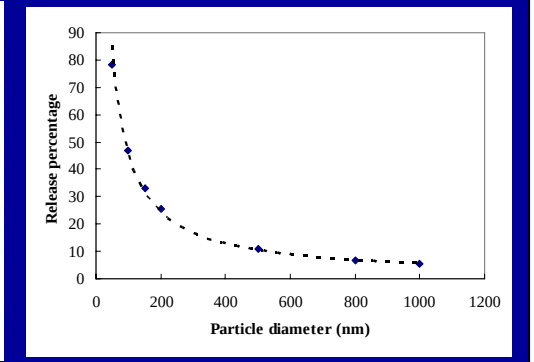

Biomed Microdevices
DOI 10.1007/s10544-008-9192-5

Iron-oxide embedded solid lipid nanoparticles for magnetically controlled heating and drug delivery

Ming-Huang Hsu · Yu-Chuan Su

Abstract This paper presents the development of magnetic lipid nanoparticles that could serve as controlled delivery vehicles for releasing encapsulated drugs in a desired manner. The nanoparticles are composed of multiple drugs in lipid matrices, which are solid at body temperature and melt around 45°C to 55°C. In addition, super-paramagnetic γ-Fe_2O_3 particles with sizes ranging from 5 to 25 nm are surface modified and dispersed uniformly in the lipid nanoparticles. In the prototype demonstration, lipid nanoparticles with average sizes between 100 and 180 nm were fabricated by high-pressure homogenization at elevated temperatures. When exposed to an alternating magnetic field of 60 kA/m at 25 kHz, a solution containing 2 g/L encapsulated γ-Fe_2O_3 particles showed a temperature increase from 37°C to 50°C in 20 min. Meanwhile, the dissipated heat melted the surrounding lipid matrices and resulted in an accelerated release of the encapsulated drugs. Within 20 min, approximately 35% of the encapsulated drug molecules were released from the lipid nanoparticles through diffusion. As such, the presented lipid nanoparticles enable a new scheme that combines magnetic control of heating and drug delivery, which could greatly enhance the performance of encapsulated drugs.

Keywords Drug delivery · Hyperthermia · Nanoparticles · Solid lipid nanoparticles · Homogenization · Magnetic heating · Controlled release

A portion of this paper was presented in the 11th International Conference on Miniaturized Systems for Chemistry and Life Sciences, Paris, France, October 2007.

M.-H. Hsu · Y.-C. Su (✉)
Department of Engineering and System Science,
National Tsing Hua University,
Hsinchu, Taiwan
e-mail: ycsu@ess.nthu.edu.tw

1 Introduction

Aiming to improve drug performance, the idea of controlled delivery with desired release profiles on specific targeted sites has been proposed since the late 1960s (Park 1997). It is commonly recognized that new drugs and novel delivery systems are equally important for achieving real progress in drug therapy (Langer 1998; Allen and Cullis 2004). By precisely controlling the concentration and distribution of a drug inside the body, potential side effects and required drug dosage could be significantly reduced, while new therapeutic schemes could be realized. Over the past few decades, there have been considerable efforts in developing various nanoparticles as effective drug delivery vehicles (Moghimi et al. 2001; Soppimath et al. 2001; Moghimi et al. 2005). By virtue of their small sizes and large surface areas covered with functionalized ligands, nanoparticles can be targeted to specific locations or cells within the body (Allen 2002; Brannon-Peppas and Blanchette 2004). Furthermore, some nanoparticles can even be activated by chemical stimuli, pH variation, remote heating, or rapidly oscillating electromagnetic field (Drummond et al. 2000; Ponce et al. 2006; Babincova et al. 2002).

Solid lipid nanoparticles, which are designed to alter the pharmacokinetics and bio-distribution of associated drugs, are particles of lipid matrices with drugs embedded and polymeric stabilizers on the surfaces (Muller et al. 2000; Mehnert and Mader 2001). In general, solid lipid nanoparticles are employed to deliver lipophilic drugs at constant rates and over long periods of time. Although continuous delivery can maintain drug concentration in a desired range to reduce adverse side effects, many situations also require, or would benefit from, a pulsatile release of drugs (Heller 1993; Redfern 2002; Stubbe et al. 2004). The reasons are mainly related to the nature of

physiological releases, in which periods of restoration of certain bodily functions between consecutive actions are often necessary. In addition, long-term administration of many potent drugs, such as those used in cancer treatments, requires drug administration at periodic intervals to avoid the poisoning of healthy tissues. To address this need, a new scheme that integrates magnetic heating elements into solid lipid nanoparticles for release control and treatment enhancement is developed. The heating is performed around 45°C to 55°C, during which solid lipid matrices are melted and the encapsulated drug molecules diffuse out of the nanoparticles. Meanwhile, the temperature rise (also described as hyperthermia [Jordan et al. 1999]) could potentially stimulate the immune response for non-specific immunotherapy of certain diseases. In such a temperature range, the functions of many proteins are modified, which in turn alters cell growth and differentiation, and could potentially induce apoptosis (Moroz et al. 2001). Traditionally, hyperthermia is performed by microwave radiation, eddy current, or dielectric heating (Hand and James 1986), but all these existing heating schemes pose serious threats to adjacent healthy tissues. Ideally, the particle-induced magnetic heating could be precisely controlled and highly localized (Sako and Hirota 1986; Pankhurst et al. 2003), and could result in no systemic effects and significantly reduced side effects in patients.

It has been demonstrated that the release of drugs from magnetoliposomes could be controlled by AC magnetic heating (Babincova et al. 2002; Viroonchatapan et al. 1998). Although the magnetoliposomes could be specifically heated to 42°C, the heating was mostly limited inside the thin lipid bi-layers. The resulting temperature rise of the magnetoliposome suspension was merely 2°C, even after 70% of the encapsulated drugs were released. Meanwhile, researchers have also demonstrated that highly concentrated magnetic nanoparticles (energized by an AC magnetic field) could result in substantial macroscopic heating of the particle suspension (Babincova et al. 2004). This paper presents a new type of delivery vehicles that can be magnetically heated to control the release of encapsulated drugs and simultaneously heat the surrounding media at a wide range of rates. Three accomplishments have been achieved: (1) fabrication of magnetic lipid nanoparticles with co-encapsulated drugs and heating elements; (2) employment of surface modified γ-Fe_2O_3 particles that can be remotely energized to activate the heating and rapid drug release; and (3) development of a new type of delivery vehicles that can achieve localized heating and pulsatile release. As such, the presented lipid nanoparticles enable a new scheme that combines magnetic control of heating and drug delivery, which could greatly enhance the performance of encapsulated drugs.

2 Operating principle

The structure of the proposed solid lipid nanoparticles is illustrated in Fig. 1. For targeted delivery, it is required to (1) pack multiple drugs and ingredients into nanoparticles with desired sizes and surface properties, and (2) couple these nanoparticles with specific ligands to guide the delivery. In this work, a lipophilic drug (tetracaine), a fluorescent dye (Nile red), and γ-Fe_2O_3 particles are dispersed in a melted lipid matrix, and the entire mixture is then emulsified in water to form solid nanoparticles once cooled down. The embedded γ-Fe_2O_3 particles, which have been widely used experimentally for numerous biomedical applications (Gupta and Gupta 2005), function as heating elements that can be remotely energized by an alternating magnetic field. Once energized, the dissipated heat melts the lipid matrices and results in an accelerated release of the encapsulated drugs.

2.1 Magnetic heating

The heating of magnetic particles in an alternating magnetic field could be attributed to various mechanisms, depending on their sizes and magnetic properties. For example, the heating in regular multi-domain ferromagnetic particles is mainly due to hysteresis losses (Andra 1998). As for nanometer-sized single-domain γ-Fe_2O_3 particles, hysteresis loss is insignificant because of the lack of domain wall. Instead, heating is caused by the rotation of the involved magnetic moments and the physical motion of the particles, in response to the alternating magnetic field (Mornet et al. 2004). Cyclically, the magnetic moments relax back to their equilibrium orientations (Neel relaxation) and dissipate the absorbed energy as heat. Meanwhile, the heating could also be due to the rotational Brownian motion within the medium. The rotational friction between the particles and the medium would result in the generation of heat around the particles. Generally, the heat dissipation is determined by the properties of particles and medium, the

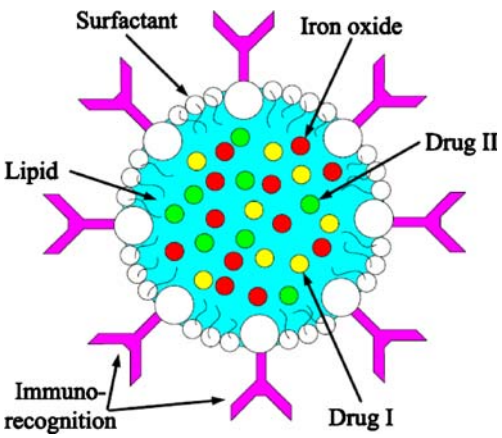

Fig. 1 Schematic illustration of the proposed solid lipid nanoparticle

geometries of particles, and the magnitude and frequency of the externally applied magnetic field (Rosensweig 2002).

2.2 Drug release

The encapsulated drugs are released by diffusing throughout the lipid nanoparticles. Consider the case that a nanoparticle with a uniform drug concentration C_0 is immersed in an infinite medium with a background drug concentration C_S, which is much lower than C_0. Driven by the concentration gradient, drug molecules diffuse from the nanoparticle to the medium. To simplify the following derivation, it is assumed that the diffusion is purely in the radial direction and the diffusion coefficient (D) is spatially invariant. Therefore, the governing equation can be expressed as

$$\frac{\partial C}{\partial t} = \nabla(D\nabla C) = \frac{1}{r^2}\frac{\partial}{\partial r}\left(Dr^2\frac{\partial C}{\partial r}\right) = D\left(\frac{\partial^2 C}{\partial r^2} + \frac{2}{r}\frac{\partial C}{\partial r}\right), \quad (1)$$

with boundary conditions

$$\begin{array}{ll} \partial C = 0, & \text{at } r = 0, \quad \text{when } t > 0 \\ C = C_S & \text{at } r = a, \quad \text{when } t > 0 \end{array}, \quad (2)$$

where $C(r)$ is the concentration profile within the nanoparticle of radius a. The diffusion equation in this case can be readily solved using Laplace transform and complex analysis methods, and the resulting analytical solution is expressed as

$$\frac{C - C_0}{C_S - C_0} = 1 + \frac{2a}{\pi r}\sum_{n=1}^{\infty}\frac{(-1)^n}{n}\sin\left(\tfrac{n\pi r}{a}\right) \times \exp\left(-\frac{n^2\pi^2 Dt}{a^2}\right) \quad (3)$$

Furthermore, the ratio of release drug mass (m) to initially packed drug mass (m_0) can be expressed as

$$f = \frac{m}{m_0} = 1 - \frac{6}{\pi^2}\sum_{n=1}^{\infty}\frac{1}{n^2}\exp\left(-\frac{n2\pi 2Dt}{a^2}\right) \quad (4)$$

Since the particle sizes, and therefore the required diffusion distances for release, are in the nanometer range, the encapsulated drugs could be released at relatively high rates even with moderate diffusion coefficients.

3 Fabrication process

3.1 Surface modification of γ-Fe_2O_3 particles

With appropriate surface coating, iron-oxide particles can be dispersed uniformly into a variety of media (Gupta and Gupta 2005). The fabrication of iron-oxide embedded solid lipid nanoparticles is illustrated in Fig. 2. First of all, 1.6 g of γ-Fe_2O_3 particles (from Aldrich) were added into 15 mL of ammonia hydroxide (30%). The mixture was vortexed and sonicated repeatedly for 3 h to facilitate the incorporation of OH groups onto particle surfaces. Afterward, γ-Fe_2O_3 particles were extracted from the mixture using a strong magnet, and rinsed with de-ionized (DI) water four times followed by dimethyl sulfoxide (DMSO) twice. The attachment of OH-groups on γ-Fe_2O_3 particle surfaces can be verified by the significant increase in the hydrophility and water solubility of the treated particles. Meanwhile, 3 mL of octadecyltrimethoxysilane (from Acros) was mixed and reacted with 20 mL of DI water at room temperature:

$$(CH_3O)_3{-}S_i - C_{18} + 3H_2O \rightarrow (HO)_3{-}S_i - C_{18} + 3CH_3OH \quad (5)$$

The mixture eventually separated into two layers, with the denser $(CH_3O)_3$–S_i–C_{18} floating on the top. Approximately 8 h later, the top $(CH_3O)_3$–S_i–C_{18} molecules were extracted and reacted with the hydroxidized γ-Fe_2O_3 particles to render their surfaces lipophilic. The reaction,

$$3Fe - OH + (HO)_3{-}S_i - C_{18} \rightarrow (Fe - O)_3{-}S_i - C_{18} + 3H_2O, \quad (6)$$

was again facilitated by repeated vortex shaking and sonication. The resulting lipophilic particles were then extracted from the mixture and rinsed with DMSO twice followed by DI water twice. At the end, the lipophilic γ-Fe_2O_3 particles were dispersed into melted lipid mixtures with required amounts at elevated temperatures.

3.2 High-pressure homogenization

The power density required to produce nanometer-sized emulsions is extremely high. It is estimated that typically a shear rate around 10^8 s^{-1} would be required to generate oil-in-water emulsions with an average droplet size around 100 nm (Taylor 1934; Mason et al. 2006). This shear rate is beyond the range of most common mixing devices, and barely achieved by few approaches such as high-pressure homogenization (Schultz et al. 2004). The key component in the homogenization process is a valve with micrometer-sized flow path as illustrated in Fig. 3. When passing through the minute gap, the fluid is highly accelerated so its pressure drops sharply. Once the pressure becomes lower than its vapor pressure, a large number of vapor bubbles nucleate inside the fluid. The multi-phase flow eventually slows down so its pressure rises, which leads to the collapse of vapor bubbles. Massive cavitational implosions are induced, and the resulting shock waves and enormous local

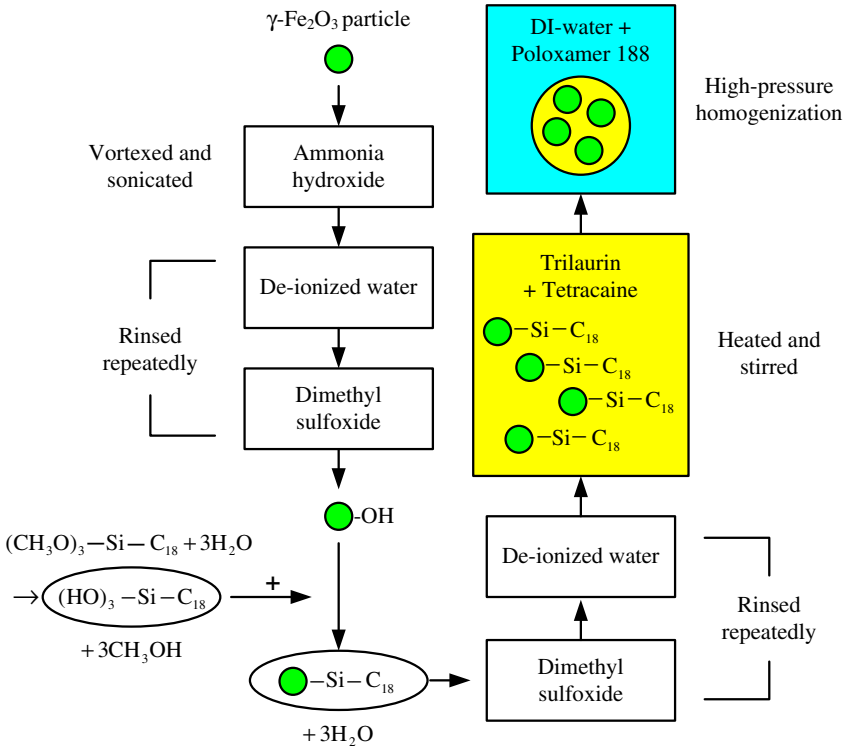

Fig. 2 Fabrication process of the proposed iron-oxide embedded solid lipid nanoparticles

temperature rise provide the required high power density for nano-emulsification (Phipps 1971; Suslick 1990). In addition, the flow-induced shear and impingement also contribute to the emulsification. At the end, the pressure drops to atmospheric pressure once the fluid reaches the outlet.

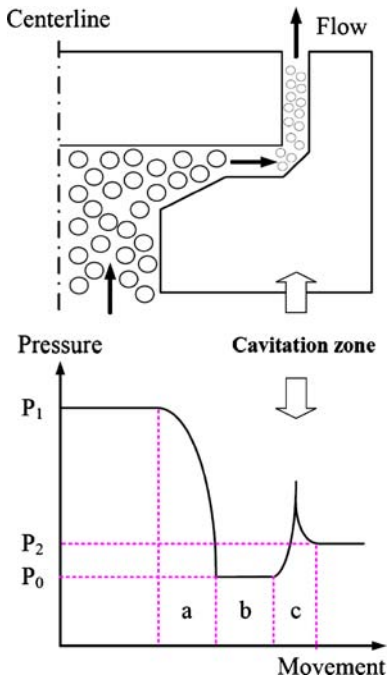

Fig. 3 Schematic illustration of the high-pressure homogenization process

The proposed solid lipid nanoparticles were prepared from trilaurin (from TCI), poloxamer 188 (from Sigma), and DI water. Five grams of γ-Fe_2O_3 embedded trilaurin was heated up to 55°C and mixed with 1 g of tetracaine (from Sigma) as the model drug. Meanwhile, 2.5 g of poloxamer 188 was dispersed into 41.5 g of DI water at 55°C. The lipid mixture was then poured into the surfactant-containing DI water and emulsified preliminarily using a disperser (HD-300, Hsiangtai) operated at 6,000 rpm for 30 min. Afterward, the lipid-in-water emulsion was further refined using a high-pressure homogenizer (Panda 2K, Niro Soavi S.p.A) at 55°C with pressures ranging from 250 to 1,000 bar and time periods between 1 and 5 min. At the end, the lipid-in-water emulsion, which contains drugs and γ-Fe_2O_3 particles inside the lipid phase, was cooled down and stored at room temperature before further heating and drug releasing trials. Because of the employment of poloxamer 188 surfactant, which stabilizes the lipid–water interface with repulsion through a steric mechanism (Moghimi and Hunter 2000), the aggregation of fabricated lipid nanoparticles was greatly eliminated.

4 Experimental details

4.1 Characterization of lipid nanoparticles

The size distribution of the fabricated lipid nanoparticles was measured using a submicron particle size analyzer

(Nicomp 380/ZLS, Particle Sizing Systems) based on dynamic light scattering. The fabricated lipid-in-water emulsion was diluted, typically from an initial volume of 200 μL to a final volume of 250 mL, before being loaded into the sample cell. Meanwhile, the concentration of γ-Fe_2O_3 encapsulated in the fabricated lipid nanoparticles was measured utilizing an atomic absorption spectrophotometer (5100PC, Perkin-Elmer). The dispersed lipid nanoparticles were filtered out of the fabricated emulsion using an aluminum oxide filter with a pore-size about 100 nm (Anodisc 25, Whatman). Roughly 20 mg of the collected, rinsed, and then dried lipid nanoparticles were re-dispersed in DI water to form a solution of 200 μL in volume. Afterward, the lipid-nanoparticle solution was mixed and reacted with 200 μL of nitric acid (70%) to dissolve the lipid matrices and release the encapsulated γ-Fe_2O_3. The released γ-Fe_2O_3 was then converted to $FeCl_3$, which can be easily ionized for concentration measurement, by adding 100 μL of 1 M hydrochloric acid into the solution. The reacted sample was further diluted to a final volume of 250 mL before being loaded into the sample cell. Meanwhile, reference solutions with known γ-Fe_2O_3 concentrations were prepared and characterized to establish the relationship between the spectrophotometer output and the corresponding γ-Fe_2O_3 concentration. Based on the measured result, the concentration of γ-Fe_2O_3 remaining in the fabricated lipid nanoparticles was estimated.

4.2 Magnetic heating and drug delivery

To characterize the magnetic heating and release control scheme, a setup (as shown in Fig. 4) including a function generator (GFG-3015, Goodwill), a high-speed power amplifier (HSA 4101, NF), and a magnetic field generator composed of a soft ferrite core wound with a 80-turn coil, were used to energize γ-Fe_2O_3 particles with an alternating magnetic field up to 60 kA/m at 25 kHz. The lipid-in-water emulsion was loaded into a microfluidic chip and observed under a microscope, or into a thermally insulated tube with an alcohol thermometer for temperature measurement. The generated magnetic field covered a space of roughly 1 × 1 × 1 cm large. Typically, colloidal samples of 1 mL in volume were placed into the field for temperature measurement. After minutes of heating, the temperatures of the colloidal solutions were recorded and analyzed.

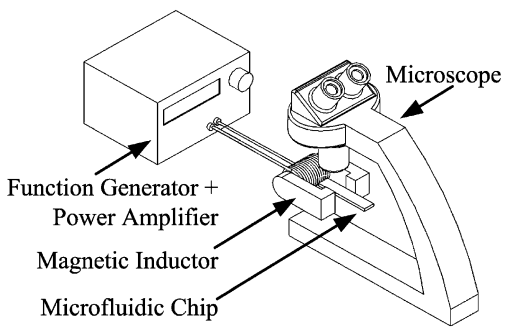

Fig. 4 Experimental setup for magnetic heating and observation

In additional to γ-Fe_2O_3 particles, tetracaine, which is a commonly used lipophilic model drug (zur Muhlen et al. 1998; Schwarz and Mehnert 1999), was co-embedded in the lipid nanoparticles. After minutes of heating, the lipid matrices were melted so tetracaine molecules could rapidly diffuse out of the nanoparticles. To characterize the release of tetracaine from the nanoparticles, the concentration of tetracaine inside the aqueous phase was measured using a UV-visible spectrophotometer (U-3300, Hitachi). Based on the measured UV absorption at 307 nm, which is proportional to the concentration of tetracaine, the release profiles of drug from the nanoparticles could be estimated. Reference solutions with known tetracaine concentrations were prepared and characterized to establish the relationship between the measured UV absorption and its corresponding tetracaine concentration. Before being loaded into the sample cell, the solid lipid nanoparticles were filtered out using aluminum oxide filters with a pore-size around 20 nm (Anodisc 25, Whatman). At the end, 200 μL of the filtered solution was diluted to a final volume of 250 mL.

5 Results and discussion

In our experiments, a lipophilic drug (tetracaine), a fluorescent dye (Nile red), and γ-Fe_2O_3 particles were co-encapsulated inside the lipid nanoparticles. After the surface treatment, the solubility of γ-Fe_2O_3 particles in melted lipid matrices was elevated to a maximum value of roughly 50 g/L. However, it was found that a large percentage of the dissolved γ-Fe_2O_3 particles separated from the melted lipid matrices during the homogenization process. As shown in Fig. 5, with an initial γ-Fe_2O_3 particle concentration of 20 g/L, roughly 65% to 40% of the particles remained in the resulting lipid nanoparticles after homogenization. The percentage decreased when higher pressures and/or longer process periods were employed. It is suspected that the relatively high density difference between γ-Fe_2O_3 and lipid might cause them to separate, when both were driven by high pressure and shock waves. The escaped γ-Fe_2O_3 particles were found to aggregate and precipitate from the solution, probably due to the lipophilicity of their surfaces. When observed under a resolution-enhanced fluorescent microscope (Cytoviva 150 on Olympus BX51), the image of the encapsulated Nile red, which are the white spots shown in Fig. 6, indicate the distribution of the fabricated lipid nanoparticles. It was

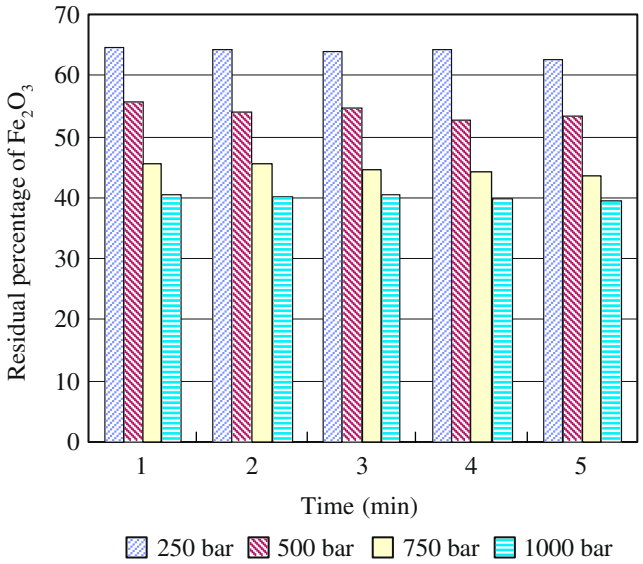

Fig. 5 Residual γ-Fe_2O_3 percentage after homogenization with various pressures and periods

found that the fabricated lipid nanoparticles distributed evenly in the aqueous solution without significant aggregation. The measured nanoparticle sizes range from 100 to 180 nm, while process pressures vary from 1,000 to 250 psi as shown in Fig. 7. It was noticed that regardless of the length of homogenization time, the resulting sizes under the same pressure were roughly the same. With an overall solution volume of 50 mL, the homogenization step was completed in 1 min, while extended processing only resulted in negligible variation in emulsion sizes. On the other hand, the lipid-to-water ratio was also found to be affecting the particle size, as shown in Fig. 8. When less lipids were dispersed into water, the size of the resulting lipid nanoparticles decreased, which may be caused by the simultaneous decrease in solution viscosity. Also shown in Figs. 7 and 8, the error bars mark the range of the mean plus and minus one standard deviation in each measurement.

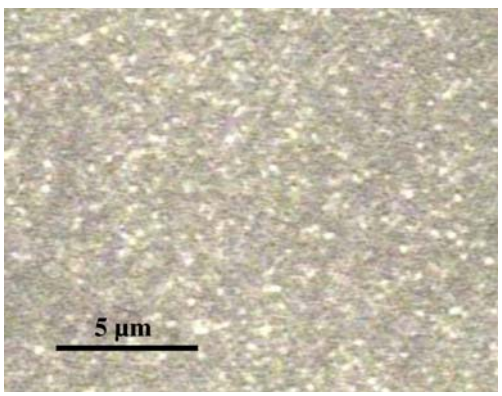

Fig. 6 Fluorescent image of the fabricated lipid-nanoparticle solution

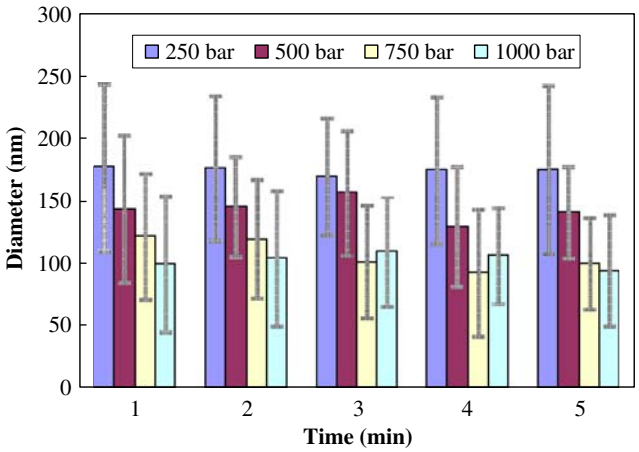

Fig. 7 Relationship between particle diameter, homogenization pressure, and process period

Nanoparticles with an average diameter of 150 nm and various γ-Fe_2O_3 concentrations were employed in our heating trials. Alcohol thermometers, which were not heated up in a magnetic field as thermocouples were, were employed to measure the temperature rise caused by magnetic heating. The magnitude of the generated magnetic field changed upon varying the frequency. With our current setup, the optimal alternating magnetic field for heating is 60 kA/m at 25 kHz. Under this field, the background temperature in the experiments was set around 37°C (body temperature) and the resulting temperature rise in the bulk solution was measured as shown in Fig. 9. The heating caused by electrical resistance and other non-magnetic mechanisms are responsible for a background temperature rise of 4°C. With lower γ-Fe_2O_3 concentration, the temperature rise was lower as expected. Among them, the maximum temperature rise achieved was 8°C (after compensation) in 20 min at a γ-Fe_2O_3 concentration of

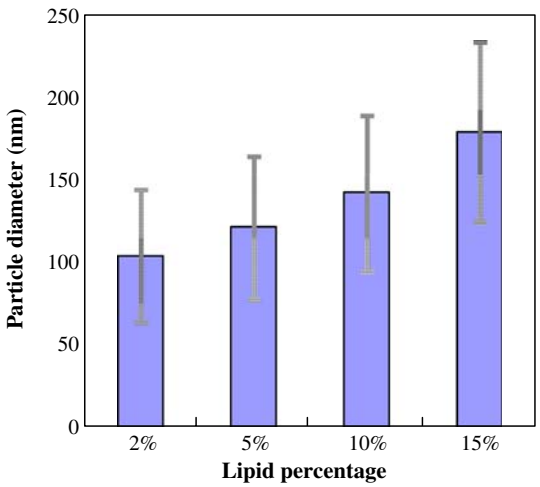

Fig. 8 Relationship between particle diameter and lipid-to-water ratio (homogenized at 500 bar)

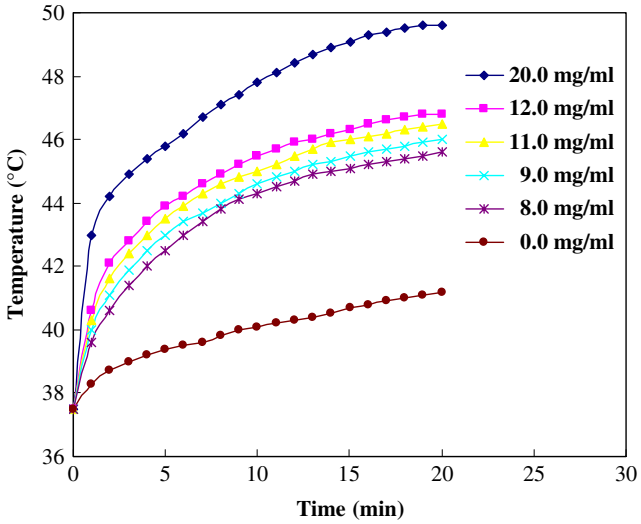

Fig. 9 Temperature profiles of solutions with various γ-Fe_2O_3 concentrations while heated

20 g/L inside the lipid nanoparticles. It is expected that the particle temperature would be much higher than the bulk solution temperature since the heat was generated therein. Under this circumstance, the heat dissipated from the embedded γ-Fe_2O_3 particles would melt the lipid nanoparticles.

In our experiments, tetracaine (with an emission wavelength at 307 nm) was employed as the model drug, whose concentration variation was measured in order to characterize the release behavior from the lipid nanoparticles. The appearance of tetracaine resulted in an absorption peak at 307 nm, whose magnitude was roughly proportional to the concentration of tetracaine. As shown in Fig. 10, the measured absorption increases sharply after short periods of heating. Based on the relationship that was calibrated as mentioned previously, the measured absorption was converted into concentration. The background concentration of tetracaine, which was measured to be about 1.3×10^{-3} M, was actually due to the leakage throughout the homogenization process. If stored at room-temperature after fabrication, the further release of tetracaine from the lipid nanoparticles would be relatively slow. For example, the overall tetracaine released throughout a 30-day period of room-temperature storage was found to be less compared to a 5-min period of magnetic heating. Because the diffusion rate across lipid matrices is higher at elevated temperatures (especially when the lipid matrices are melted), a highly accelerated release of the encapsulated tetracaine was observed as expected. It was measured that after a 20-min period of heating, roughly 35% of the original encapsulated tetracaine was released from the lipid nanoparticles as shown in Fig. 11. Based on the simplified diffusion model (whose analytical solutions are expressed as Eqs. 3 and 4), a numerical simulation with measured parameters including $C_0=6.5\times10^{-2}$ M, $C_S=1.3\times10^{-3}$ M, a=75 nm, and $D=5.8\times10^{-20}$ m^2/s was performed. Among these parameters, the diffusion coefficient (D) of tetracaine molecules across melted lipid matrices was measured at 48°C. Compared with the release profile predicted by the simplified model, the measured one shows less variation in its slope (release rate) over the 20-min period, as illustrated in Fig. 11. Ideally, the release rate decreases over time because of the

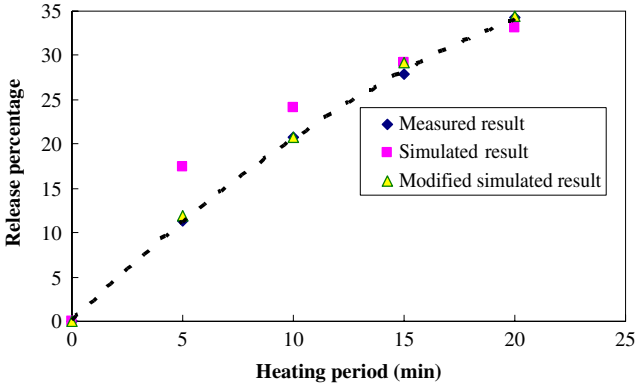

Fig. 11 Drug release profiles of measured and simulated results

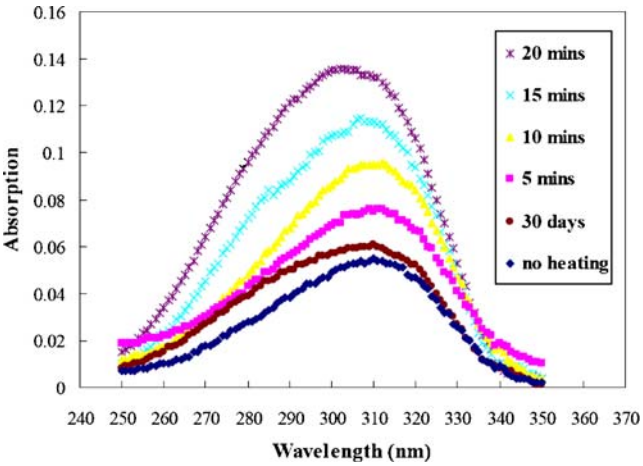

Fig. 10 UV absorption curves after magnetic heating with various periods

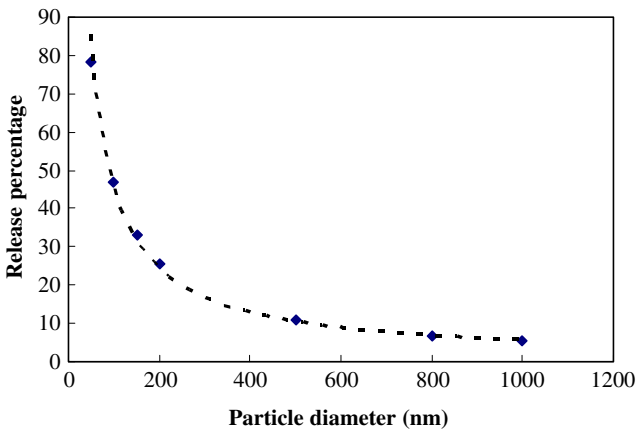

Fig. 12 Simulated drug-release percentage in 20 min with various particle sizes

reduction in concentration gradient. The reason for this deviation is probably the temperature dependency of the diffusion coefficient (D), which is low at the beginning of the heating period and increases following the temperature rise. Employing a temperature-dependent diffusion coefficient in the simulation should greatly reduce this deviation. For example, if values of 50%, 75%, 100%, and 110% of the diffusion coefficient measured at 48°C are employed to estimate the drug diffusion during the periods from 0 to 5, 5 to 10, 10 to 15, and 15 to 20 min, respectively, the simulated result matches the measured one with a deviation less than 10% as indicated in Fig. 11. In another trial, solutions with half of the lipid nanoparticle concentration (5%) were magnetically heated. It was measured that the temperature rise was 5°C lower than the 10% ones, while the release percentage dropped from 35% to 30% (roughly a 15% drop). To better explain the release characteristics of the proposed lipid nanoparticles, a detailed model considering the temperature and spatial dependency of the drug diffusion process would be needed.

Another crucial factor for the observed rapid release is the size of the lipid nanoparticles. Based on our simulation with various particle sizes as shown in Fig. 12, the release percentage in 20 min could be elevated from 35% to 50% and 75% when particles of 100 and 50 nm in diameters are employed, respectively. Since the required diffusion distance is shorter when drug molecules diffuse across a smaller particle, the drug-release percentage of a smaller particle is expected to be higher than that of a large one in the same diffusion period. It is predicted that the purely diffusion-induced release varies inversely with the particle size (as indicated in Fig. 12), while further experimental verification is required. Although the drug release from microparticles is estimated to be slow using the simplified diffusion model, the actual experimentally determined release rates are surprisingly high in many cases (Liggins and Burt 2001; Siepmann et al. 2004; Arifin et al. 2006). For example, the drug release from PLGA-based microparticles is accelerated by the so-called autocatalytic effects (Siepmann et al. 2005), which significantly reduce the difference in the release rates between PLGA micro- and nanoparticles. Meanwhile, it is expected that if further heating is performed, the drug-release rate decreases monotonously with the decrease in concentration gradient. It is estimated by the simplified model that for particles of 150 nm in diameters, the release percentage in the first, second, and third 20-min periods will be roughly 35%, 12%, and 8%, respectively. It would require roughly 2 h of heating to achieve a release percentage of 70%. Over an extended period of time, all the encapsulated drug molecules will be released by either diffusion (with or without heating) or the degradation of lipid matrices.

6 Conclusion

We have successfully demonstrated the fabrication, magnetic heating, and controlled release of the proposed solid lipid nanoparticles. The nanoparticles are composed of multiple drugs in lipid matrices, which are solid at body temperature and melt around 45°C to 55°C. In addition, super-paramagnetic γ-Fe_2O_3 particles with diameters ranging from 5 to 25 nm are surface modified and distributed uniformly in the lipid nanoparticles. In the prototype demonstration, lipid nanoparticles with average diameters between 100 and 180 nm were fabricated by high-pressure emulsification at elevated temperatures. The maximum γ-Fe_2O_3 concentration inside the resulting lipid nanoparticles was 20 g/L, while a large percentage of the dissolved γ-Fe_2O_3 particles separated from the melted lipid matrices during the homogenization process. When exposed to an alternating magnetic field of 60 kA/m at 25 kHz, a solution containing 2 g/L encapsulated γ-Fe_2O_3 particles showed a temperature rise from 37°C to 50°C in 20 min. Meanwhile, the dissipated heat melted the lipid matrices and resulted in an accelerated release of the encapsulated drugs. In the 20-min period, roughly 35% of the drug molecules that were initially encapsulated in the lipid nanoparticles (150 nm in diameter) were released through diffusion. Based on our simulation, the release percentage in 20 min could be elevated from 35% to 50% and 70% when particle sizes of 100 and 50 nm are employed, respectively. In another trial, solutions with half of the lipid-nanoparticle concentration (5%) were magnetically heated, and the resulting temperature rise was 5°C lower than the 10% ones, while the release percentage dropped slightly from 35% to 30%. As such, the presented lipid nanoparticles enable a new scheme that combines magnetic control of heating and drug delivery, which could greatly enhance the performance of encapsulated drugs.

Acknowledgements The demonstrated systems were fabricated in the ESS Microfabrication Lab at National Tsing Hua University, Taiwan. This work was supported in part by the National Science Council of Taiwan under Contract no. NSC 96-2221-E-007-116-MY3.

References

T.M. Allen, Nat. Rev. Cancer **2**, 750 (2002)
T.M. Allen, P.R. Cullis, Science **303**, 1818 (2004)
W. Andra, in Magnetism in Medicine: A Handbook, ed. by W., Andra, H., Nowak (Wiley-VCH, Berlin, 1998)
D.Y. Arifin, L.Y. Lee, C.H. Wang, Adv. Drug Deliv. Rev. **58**, 1274 (2006)
M. Babincova, P. Cicmanec, V. Altanerova, C. Altaner, P. Babinec, Bioelectrochemistry **55**, 17 (2002)
M. Babincova, V. Altanerova, C. Altaner, P. Cicmanec, P. Babinec, Med. Phys. **31**, 2219 (2004)

L. Brannon-Peppas, J.O. Blanchette, Adv. Drug Deliv. Rev. **56**, 1649 (2004)
D.C. Drummond, M. Zignani, J.C. Leroux, Prog. Lipid Res. **39**, 409 (2000)
A.K. Gupta, M. Gupta, Biomaterials **26**, 3995 (2005)
J.W. Hand, J.R. James, *Physical Techniques in Clinical Hyperthermia* (Wiley, New York, 1986)
J. Heller, Crit. Rev. Ther. Drug Carr. Syst. **10**, 253 (1993)
A. Jordan, R. Scholz, P. Wust, H. Fahling, R. Felix, J. Magn. Magn. Mater. **201**, 413 (1999)
R. Langer, Nature **392S**, 5 (1998)
R.T. Liggins, H.M. Burt, Int. J. Pharm. **222**, 19 (2001)
T.G. Mason, J.N. Wilking, K. Meleson, C.B. Chang, S.M. Graves, J. Phys. Condens. Mater. **18**, R635 (2006)
W. Mehnert, K. Mader, Adv. Drug Deliv. Rev. **47**, 165 (2001)
S.M. Moghimi, A.C. Hunter, Trends Biotechnol. **18**, 412 (2000)
S.M. Moghimi, A.C. Hunter, J.C. Murray, Pharmacol. Rev. **53**, 283 (2001)
S.M. Moghimi, A.C. Hunter, J.C. Murray, FASEB J. **19**, 311 (2005)
S. Mornet, S. Vasseur, F. Grasset, E. Duguet, J. Mater. Chem. **14**, 2161 (2004)
P. Moroz, S.K. Jones, B.N. Gray, J. Surg. Oncol. **77**, 259 (2001)
R.H. Muller, K. Mader, S. Gohla, Eur. J. Pharm. Biopharm. **50**, 161 (2000)
Q.A. Pankhurst, J. Connolly, S.K. Jones, J. Dobson, J. Phys. D. Appl. Phys. **36**, R167 (2003)
K. Park, *Controlled Drug Delivery: Challenges and Strategies* (American Chemical Society, Washington, DC, 1997)
L.W. Phipps, Nature **233**, 617 (1971)
A.M. Ponce, Z. Vujaskovic, F. Yuan, D. Needham, M.W. Dewhirst, Int. J. Hyperthermia **22**, 205 (2006)
P.H. Redfern, Drug Deliv. Syst. Sci. **2**, 21 (2002)
R.E. Rosensweig, J. Magn. Magn. Mater. **252**, 370 (2002)
M. Sako, S. Hirota, Gan To Kagaku Ryoho **13**, 1618 (1986)
C. Schwarz, W. Mehnert, J. Microencapsul. **16**, 205 (1999)
S. Schultz, G. Wagner, K. Urban, J. Ulrich, Chem. Eng. Technol. **27**, 361 (2004)
J. Siepmann, N. Faisant, J. Akiki, J. Richard, J.P. Benoit, J. Control. Release **96**, 123 (2004)
J. Siepmann, K. Elkharraz, F. Siepmann, D. Klose, Biomacromolecules **6**, 2312 (2005)
K.S. Soppimath, T.M. Aminabhavi, A.R. Kulkarni, W.E. Rudzinski, J. Control. Release **70**, 1 (2001)
B.G. Stubbe, S.C. De Smedt, J. Demeester, Pharm. Res. **21**, 1732 (2004)
K.S. Suslick, Science **247**, 1439 (1990)
G.I. Taylor, Proc. R. Soc. Lond. A. **146**, 501 (1934)
E. Viroonchatapan, H. Sato, M. Ueno, I. Adachi, J. Murata, I. Saiki, K. Tazawa, I. Horikoshi, J. Drug Target. **5**, 379 (1998)
A. zur Muhlen, C. Schwarz, W. Mehnert, Eur. J. Pharm. Biopharm. **45**, 149 (1998)